Chemical Science

ROYAL SOCIETY OF CHEMISTRY

EDGE ARTICLE

View Article Online
View Journal | View Issue

Cite this: *Chem. Sci.*, 2025, **16**, 8092

All publication charges for this article have been paid for by the Royal Society of Chemistry

Received 2nd December 2024
Accepted 26th March 2025

DOI: 10.1039/d4sc08179j

rsc.li/chemical-science

Series of Geländer oligomers with orthogonal rungs†

Adriano D'Addio, [a] Camiel C. E. Kroonen, [a] Olaf Fuhr, [b] Dieter Fenske, [b] Daniel Häussinger [a] and Marcel Mayor *[abc]

The synthesis and analyses of a series of "Geländer" oligomers with perpendicularly arranged rungs are reported. The synthesis is achieved by forming the axis with a statistical end-capped oligomerization, before the banister is wrapped around it by Eglinton couplings. The intrinsic helical chiral structures are characterized by NMR spectroscopy and mass- and photo spectrometry, and for the trimer, even the solid-state structure is determined. The dimeric, trimeric, and tetrameric structures are resolved into their enantiomers and their electronic circular dichroism is studied.

Introduction

Linking adjacent repeating units of oligophenylenes with an elongated tether to each other leads to molecular architectures reminiscent of the banister (or "Geländer" in German) of a spiral staircase as the longer stringer needs to wrap helically around the shorter stringer.[1–10] Studies on length-dependent properties of "Geländer" oligomers, especially regarding their chiroptical activity, are limited. There is a plethora of tethered biphenylenes and tolanes that can be considered as banister dimers,[3,7,11–14] and few examples of trimers,[1,2,4–6,8–10] and we found only one reported example of a tetramer[15] and a pentamer.[4]

The early examples of trimeric and pentameric banisters led to an excessive number of possible isomers. Trimeric structures bear two stereogenic axes leading to two chiroptically active isomers and one chiroptically mute *meso* isomer.[1] The pentameric structure has four stereogenic axes, which can assume different configurations leading up to 10 isomers that were not resolved.[4] By introducing a size mismatch design principle, this limitation is overcome and the complexity of the stereochemistry is reduced to just two configurations: (*M*) and (*P*). Even though the total number of stereogenic axes is not reduced,[16] the increased mechanical rigidity entangles the axis to assume the same configuration. In the initial endeavors of our group, the "Geländer" structures were resolved into their (*M*) and (*P*) isomers and displayed racemization at room temperature with racemization barriers of comparable dimensions to Vögtle's pioneering "Geländer"-trimers.[1,2]

The synthesis of elongated systems was limited due to a lack of regioselectivity during geländerfication (the reaction step where the banister is formed), which formed two constitutional isomers of the banister structures.[6,9] The unfavorable selectivity arises from free rotation along the rung, leading to distortion of the banister in structures based on 60° angles between the axis, rung, and banister.[6] This limited our endeavors so far to the preparation of "Geländer"-trimers. A possible solution is a stepwise geländerfication.[8] An apparent drawback is the increased demand for synthetic steps and limited orthogonal protection and masking strategies.[17] Another approach is introducing 90° rungs, where the rungs can freely rotate without leading to constitutional isomers. Recently, we reported a dimeric structure with a novel banister design based on orthogonal angles connecting the axis, rung, and banister (Fig. 1).[18] "Geländer"-type structures with efficiently conjugated helical banisters are even less accessible. Our efforts either showed optically inefficient conjugation or they suffered from limited stability.[7,8,15] Effective π-conjugated banisters promise chiroptical activity from the helically wrapped chromophore and hopefully will also soon allow the investigation of transport phenomena along helically twisted pathways. Helical chiral π-conjugated materials are not only promising for potential spintronic devices, but they are perfect prospects for tailoring chiroptical properties, which is a design factor of future OLED (organic light emitting diode) devices or as an additional feature in sensing applications.[19–21]

"Geländer" oligomers based on orthogonal rungs are not only characterized by high racemization barriers and a conjugated banister, but the orthogonal arrangement of its subunits makes it ideally suited to develop elongated oligomers in order to study structure–property correlations that have not been accessible before.

[a]*Department of Chemistry, University of Basel, St. Johanns-Ring 19, Basel, 4056, Switzerland. E-mail: marcel.mayor@unibas.ch*

[b]*Institute for Nanotechnology (INT) and Karlsruhe Nano Micro Facility (KNMFi), Karlsruhe Institute of Technology (KIT), P. O. Box 3640, Karlsruhe, 76021, Germany*

[c]*Lehn Institute of Functional Materials (LIFM), School of Chemistry, Sun Yat-Sen University (SYSU), Guangzhou, 510275, China*

† Electronic supplementary information (ESI) available. CCDC 2378167. For ESI and crystallographic data in CIF or other electronic format see DOI: https://doi.org/10.1039/d4sc08179j

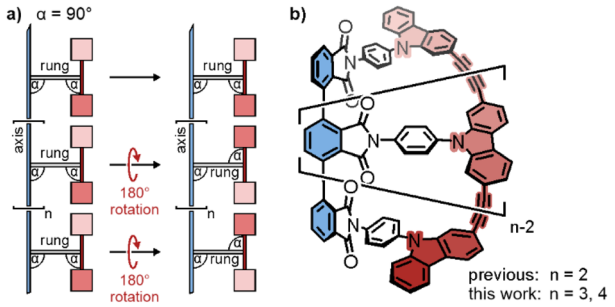

Fig. 1 (a) Concept: 90° angles α between the axis, rungs, and banister avoid regioselectivity challenges during geländerfication. (b) Structure of the "Geländer" oligomers with the desired 90° angles.

Synthesis

Retrosynthetic analysis of such oligomers reveals two sequential homocoupling reactions. An oxidative acetylene homocoupling is envisioned for the geländerfication[22] and a Yamamoto-type end-capped oligomerization to build up the axis (Scheme 1). Suitable monomers $\mathbf{M_X}$ and endcaps $\mathbf{EC_X}$ can be synthesized in a few steps from 2,7-dibromocarbazole, 3,6-dihalido phthalic anhydride, 2-bromo carbazole, 3-halido phthalic anhydride, and 4-fluoro nitrobenzene, respectively. The halide can be quickly exchanged for the Yamamoto-type coupling by choosing the appropriate phthalic anhydride. The synthesis of $\mathbf{M_X}$ is similar to the reported synthesis of $\mathbf{EC_{Br}}$.[18] Substitution of fluorine in 4-fluoro nitrobenzene with the nitrogen of 2,7-dibromo-9*H*-carbazole performed excellently in a solution of DMSO (dimethyl sulfoxide) in the presence of caesium fluoride in yields up to 98%. Substituted product **2** was readily precipitated with deionized water as a mustard yellow powder and collected by filtration, slightly darker in shade than its monobromo derivative **1**. Excess 4-fluoronitrobenzene, residual caesium fluoride, and residual DMSO were removed by washing the crude product with deionized water and warmed diethyl ether. Subsequently, the masked alkynes were installed by a Sonogashira–Hagihara coupling, and compound **4** was isolated after normal phase column chromatography in a yield of 92% as a yellow powder. In the presence of $SnCl_2$ in a mixture of ethanol and tetrahydrofuran (THF), the nitro group in **4** was reduced to an amine, which after aqueous workup allowed us to obtain **6** in sufficiently high purity as determined by ^{1}H-NMR, and it was directly submitted to the next step without any further purification.

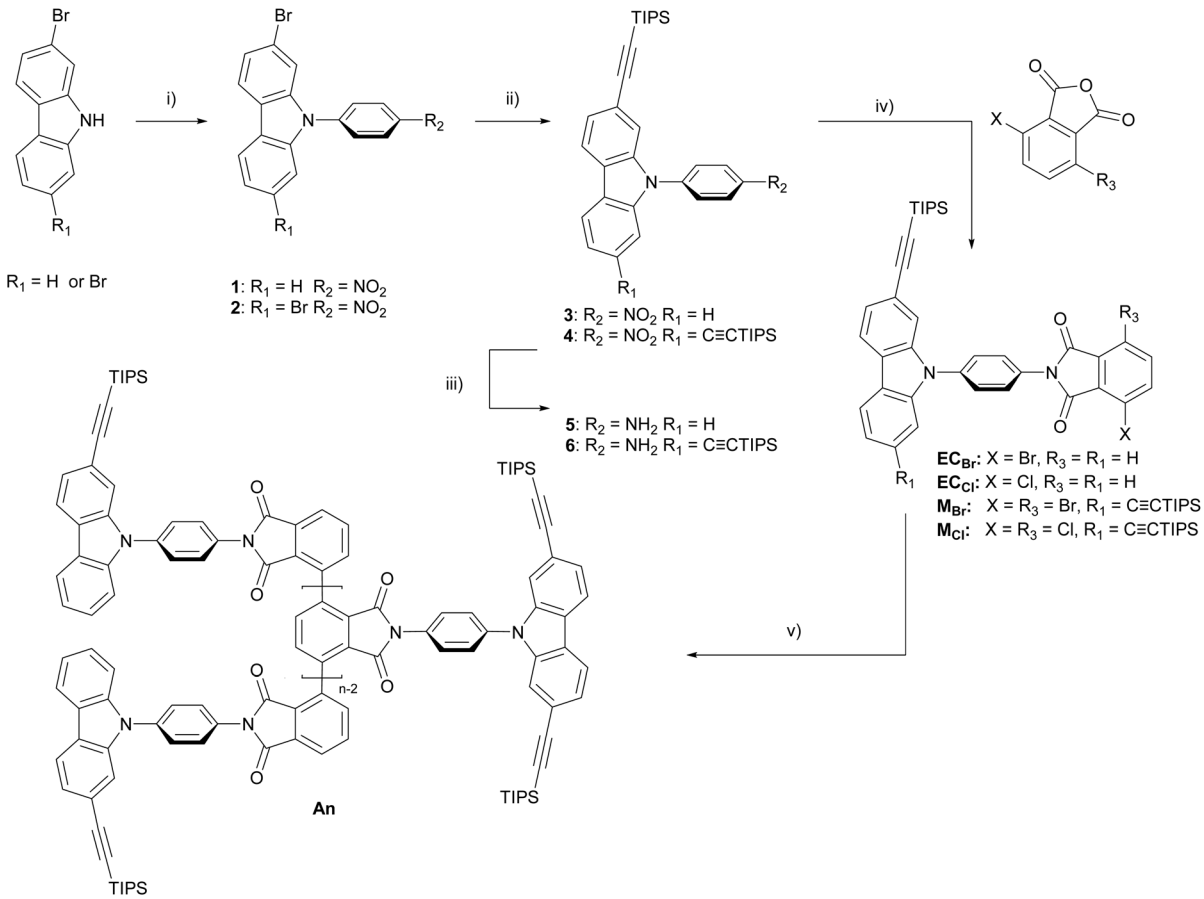

Scheme 1 Synthetic pathway to oligomers **An**. Reagents and conditions: (i) CsF, 4-fluoro nitrobenzene, DMSO, 150 °C, 20 h, 1: 92%, 2: 98%; (ii) HCCSi(C.H. $(CH_3)_2)_3$, $Pd(PPh_3)_4$, CuI, DIPA, THF, 90 °C, 20 h, 3: 94%; 4: 92%; (iii) $SnCl_2$, THF, EtOH, 50 °C, 20 h; (iv) 3-bromophthalic anhydride or 3-chlorophthalic anhydride, AcOH, 70 °C or 120 °C, 48 h or 24 h; $\mathbf{EC_{Br}}$ 84%, $\mathbf{EC_{Cl}}$ 83% $\mathbf{M_{Br}}$ 78% and $\mathbf{M_{Cl}}$ 92% isolated yield over both steps (iii) and (iv). (v) Method A: $NiBr_2$, Zn, PPh_3, DMAc, 80 °C, 20 h; method B: $Ni(PPh)_3Cl_2$, Zn, PPh_3, KI, THF or 2-MeTHF, 80 °C, 20 h.

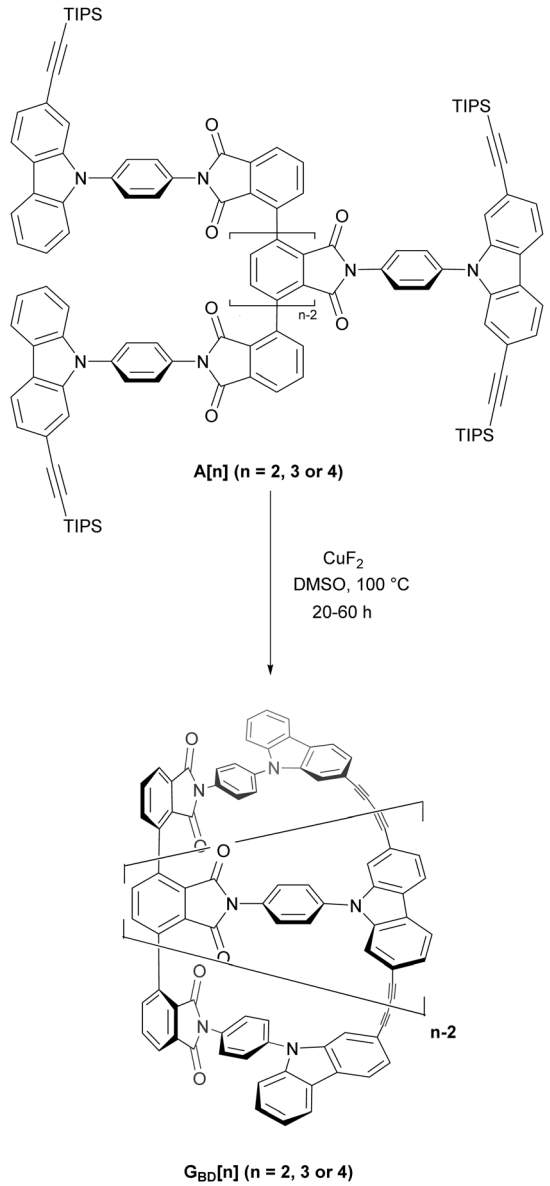

Scheme 2 Geländerfication of A[2], A[3], and A[4] by Eglington coupling.

3,6-Dibromo phthalic anhydride was allowed to react with the amine **6** in acetic acid to give $\mathbf{M_{Br}}$ in a yield of 78% over two steps. $\mathbf{EC_{Cl}}$ and $\mathbf{M_{Cl}}$ were synthesized analogously using the corresponding chlorophthalic anhydride, allowing us to obtain $\mathbf{EC_{Cl}}$ in 83% and $\mathbf{M_{Cl}}$ in 92%, both over two steps. Interestingly, changing to chloro phthalic anhydrides required higher temperatures. The obtained solids were fainter in color than their corresponding bromo derivatives. With the monomers $\mathbf{M_X}$ and the endcaps $\mathbf{EC_X}$, the oligomerization to **A[*n*]** was investigated. In analogy to the work of Wasilewski and co-workers,[23] the product distribution was assumed to depend on the stoichiometry of the starting materials. The first focus was set on the trimer **A[3]** – therefore, two equivalents of $\mathbf{EC_{Br}}$ were reacted with one equivalent of $\mathbf{M_{Br}}$ in a statistical reductive coupling in the presence of $NiBr_2$, Zn, and PPh_3 in dimethyl acetamide (DMAc). To our delight, we observed the formation of oligomers by MALDI-ToF-MS and were able to isolate **A[2]** (27%), **A[3]** (11%), **A[4]** (4%), and **A[5]** (1%) by preparative GPC (gel-permeation chromatography). Attempts to improve this reductive coupling turned out to be challenging. Not only the number of variables that have to be considered, but also their sensitivity to not yet identified boundary conditions prevented a substantial improvement of the oligomer yields (attempts described in the ESI†). We thus accepted the overall moderate isolated yield of 43% and moved our attention to the next challenge, geländerfication. Analysis of the isolated oligomers **A[*n*]** by ^{1}H-NMR spectroscopy readily determined the number of repeating units, as the signal of the tri(*iso*)propyl silane of the terminal carbazoles is downfield shifted compared to that of tri(*iso*)propyl silane in the repeating units (see ESI, Fig. S2†), as the repeating units are more shielded being neighboured by two carbazole units while the endcap is only in the vicinity of one other carbazole. Due to the limited quantity of available material, the focus was set on the reaction from **A[3]** to $\mathbf{G_{BD}[3]}$, and from **A[4]** to $\mathbf{G_{BD}[4]}$, respectively (Scheme 2).

The deprotection of the alkynes and their oxidative coupling to the 1,3-butadiyne linker were performed in the same reaction benefitting from the double role of copper fluoride (CuF_2). The reagent provides fluoride ions to liberate the alkynes and copper ions acting as a catalyst for the oxidative alkyne coupling. The starting materials were stirred vigorously in aerated DMSO at 100 °C in the presence of CuF_2 for three days. The crude product was precipitated with deionized water, and the solids were collected. Further purification by preparative GPC provided isolated yields of 44% for $\mathbf{G_{BD}[3]}$ and 35% for $\mathbf{G_{BD}[4]}$, respectively. Even though geländerfication of the small amounts of **A[5]** available was attempted and the mass $\mathbf{G_{BD}[5]}$ could be observed, isolation failed.

Structural analysis

^{1}H-NMR of $\mathbf{G_{BD}[3]}$ (Fig. 2) displayed all expected signals with a pronounced broadening of the AB-system of the phenylene

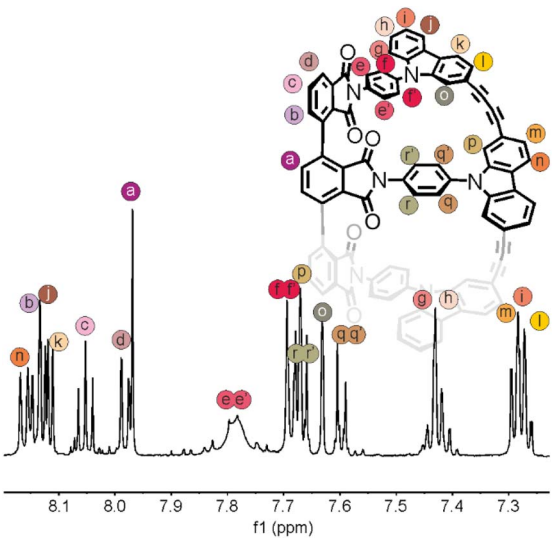

Fig. 2 ^{1}H-NMR of $\mathbf{G_{BD}[3]}$ recorded at 298 K. The colored points labeled with small letters assign the ^{1}H-NMR signals to the corresponding protons of the "Geländer" structure.

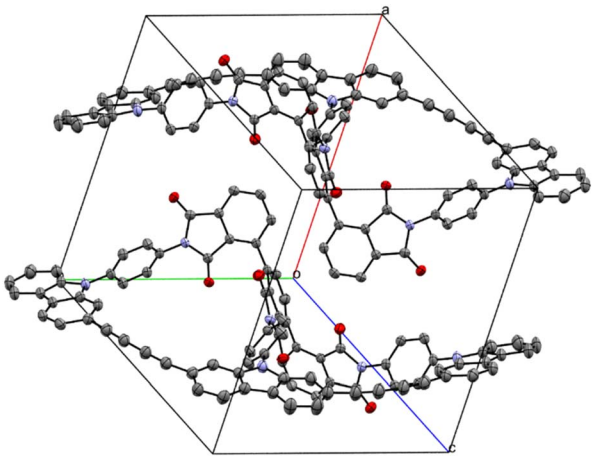

Fig. 3 Both enantiomers of the solid-state structure of (*rac*)-G_{BD}[3] in their unit cell: hydrogens and solvents were omitted for clarity. ORTEP ellipsoids are displayed at a 50% probability. Top: (*M*)- and bottom: (*P*)-G_{BD}[3].

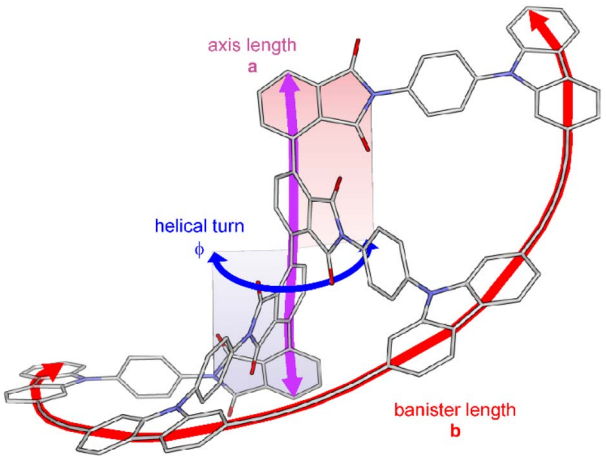

Fig. 4 Wireframe model of (*P*)-G_{BD}[4] together with the geometric values summarized in Table 1. Hydrogens are omitted for clarity.

sub-units connecting the axis and banister (rungs), which disappears upon elevating the NMR-recording temperature to 333 K (see the ESI†). Interestingly, it seems that the rungs of the endcapping units are more rotationally hindered than the central rung. In addition to the characterization by high-resolution mass spectrometry (HRMS), single crystals suitable for X-ray diffraction experiments were obtained by slow evaporation of the NMR-sample (d8-THF) at 7 °C. The solid-state structure of (*rac*)-**G_{BD}[3]** is displayed in Fig. 3. The racemate crystallized in the $P\bar{1}$ space group surrounded by eight THF molecules. The unit cell consists of one (*M*)-**G_{BD}[3]** and one (*P*)-**G_{BD}[3]** moiety.

The limited availability of racemic **G_{BD}[4]** restricted its NMR characterization to HSQC (heteronuclear single quantum coherence) experiments displaying the proton-bearing carbons. The identity of the compound was corroborated by ^{1}H-NMR spectroscopy and HRMS.

Further insights were gleaned from computational modeling optimizing the geometries of **G_{BD}[2]**, **G_{BD}[3]** and **G_{BD}[4]** at the B3LYP/def2-SVP level of theory. Benchmarking the *in vacuo* optimized geometry of **G_{BD}[3]** with its solid-state structure displayed only minute differences. Even the slightly smaller helical turn in the optimized model (135.2°) compared to the X-ray structure (138.2°) is minute considering the different boundary conditions of both experiments and points at the structural persistence of the "Geländer" architecture. All attempts to grow single crystals of **G_{BD}[4]** failed so far, but its *in vacuo* calculated structure is displayed in Fig. 4. The repetitive nature of these "Geländer" oligomers enabled not only the prediction of structural features by compounding the corresponding subunits from the solid-state structure of the dimer **G_{BD}[2]**, but also the comparison of the oligomers' subunits with each other. As summarized in Table 1, the rigid nature of the banister and the axis is revealed, as indicated by the length of the axis (violet arrow in Fig. 4) and the length of the banister (red arrow in Fig. 4). Both distances extracted from the models of **G_{BD}[3]** and **G_{BD}[4]** and from the X-ray structure of **G_{BD}[3]** deviate only minutely from the expectation extrapolated from the X-ray structure of **G_{BD}[2]**. Interestingly, the extracted helical turns (blue arrow in Fig. 4) are larger for any structures of **G_{BD}[3]** and **G_{BD}[4]** than the extrapolation from either the model or solid-state structure of **G_{BD}[2]**. It seems that the elongation of the banister results in a slightly less bent arrangement of the 1,3-butadiene linkers. The most characteristic feature of "Geländer" structures is their helicity. During geländerfication, the banister is expected to wind helically around the axis, forming a (*P*) and an (*M*) isomer in a racemic mixture. The

Table 1 Comparison of selected structural features predicted by the calculated models and X-ray structures

	G_{BD}[2] X-ray	**G_{BD}[3]** X-ray	**G_{BD}[2]** model	**G_{BD}[3]** model	**G_{BD}[4]** model
Axis length a	7.17 Å	11.43 Å	7.23 Å	11.60 Å	15.96 Å
Banister length b	20.07 Å	33.49 Å	20.33 Å	33.79 Å	46.63 Å
Helical turn Φ	62.52°	138.19°	66.11°	135.18°	203.23°
Helical turn[a] per repeat unit $\Phi/(n-1)$		69.01°[b]		67.59°	66.28°[c]
		69.18°[b]			66.30°[d]
					70.67°[e]

[a] The models are calculated devoid of a solvent and therefore the torsions are symmetric from the center while residual solvent induces minute changes in the solid-state structure. [b] The same torsions are observed in the *P* and *M* isomers. [c] The torsion angles between the third and fourth subunits, respectively. [d] The torsion angles between the first and second subunits, respectively. [e] The torsion angle between the second and third subunits.

enantiomers were resolved using chiral stationary phase HPLC (separation protocols are provided in the ESI†). As all the used stationary phases are based on similar functionalized sugar polymers, we hypothesized that in analogy to **G_{BD}[2]**, the first eluted isomers are (*P*)-**G_{BD}[3]** and (*P*)-**G_{BD}[4]**, respectively.

And indeed, the comparison of the recorded electronic circular dichroism (ECD) spectra with their simulated spectra with the rotary strength computed at the TD-PBE0/def2-SVP level of theory (see the ESI for computational details and Fig. S9 and S10† for comparison of the spectra) corroborated the assignment.

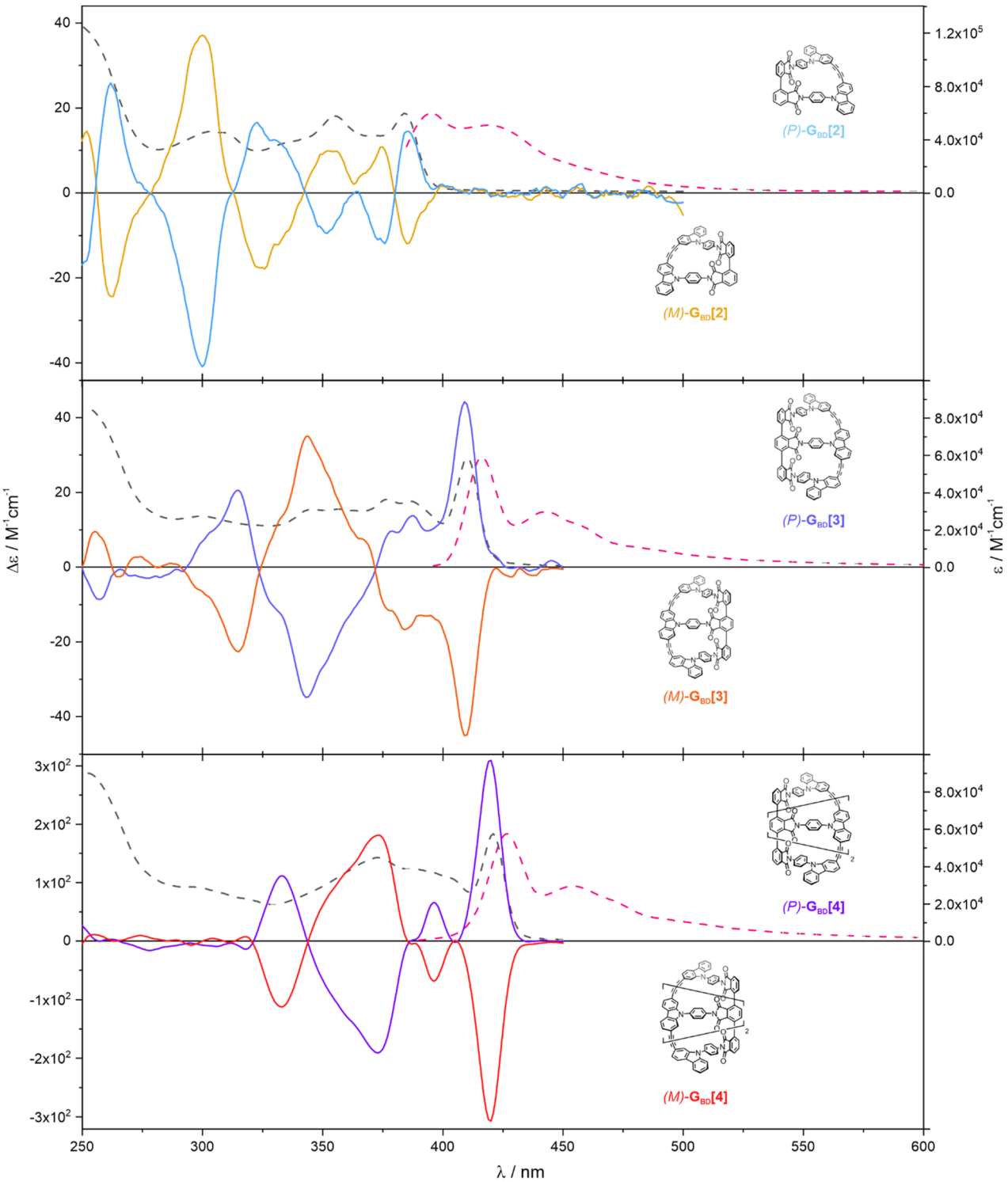

Fig. 5 ECD spectra of all resolved enantiomers of G_{BD}[2] (top), G_{BD}[3] (middle), and G_{BD}[4] (bottom). The absorption spectra are displayed as black dashed lines, and normalized emission spectra are displayed as magenta dashed lines. All measurements were collected in $CHCl_3$ at $c = 10^{-6}$ M. The assignment of helicity was corroborated by comparison to the simulation ECD spectra.

Optical analysis

$\mathbf{G_{BD}[2]}$, together with the herein-reported $\mathbf{G_{BD}[3]}$ and $\mathbf{G_{BD}[4]}$, are the first series of enantiomerically stable "Geländer" structures comprising a conjugated banister. Of particular interest was thus their optical and especially, their chiroptical properties. As displayed in Fig. 5, a significant red-shift of the absorption maximum from 386 nm in $\mathbf{G_{BD}[2]}$ to 410 and 420 nm for $\mathbf{G_{BD}[3]}$ and $\mathbf{G_{BD}[4]}$, respectively, was observed (dashed black lines in Fig. 5). The conjugation in the banister becomes apparent by considering that their precursors $\mathbf{A_2}$, $\mathbf{A_3}$, and $\mathbf{A_4}$ displayed exclusive absorption below 375 nm (see ESI, Fig. S2†).

The emission spectra of $\mathbf{G_{BD}[3]}$ and $\mathbf{G_{BD}[4]}$ are of similar shape to the one of $\mathbf{G_{BD}[2]}$ (dashed magenta lines in Fig. 5), with the higher wavelength peaks becoming less pronounced with increasing oligomer extension. As comparable variations of the mirrored signals are observed in the corresponding absorption spectra, the feature originates from the Franck–Condon principle. The emissions of the individual banister structures are equidistantly red-shifted like the absorption spectra without a significant change in absorptivity. Also, the intercept of the normalized absorption and emission spectra red-shifts, documenting the expected decrease of the optical HOMO–LUMO energy gap ($E_{0\text{–}0}$) with increasing banister length.

The ECD spectra of the separated isomers are displayed in Fig. 5. As expected, the ECD spectra of the (*P*) and (*M*) isomers of the oligomers $\mathbf{G_{BD}[2]}$, $\mathbf{G_{BD}[3]}$, and $\mathbf{G_{BD}[4]}$ are perfect mirror images of each other, with all Cotton bands of opposite signs. While the most intense Cotton band for $\mathbf{G_{BD}[2]}$ is at around 300 nm, a region where the axis dominates the absorption spectrum, the most intense Cotton bands of $\mathbf{G_{BD}[3]}$ and $\mathbf{G_{BD}[4]}$ are both red-shifted to above 400 nm where the absorption spectrum arises from extended conjugation in the carbazole subunits. A red-shift of the Cotton bands with increasing banister length is observed, together with an increase in the dissymmetry factor g_{abs} ($g_{abs} = |\Delta\varepsilon/\varepsilon|$, see Table 2), which is an indicator of the chiroptical spectral quality. Such features have already been reported for helicenes.[24,25] Also it was hypothesized in the pioneering work of Kiupel *et al.* for "Geländer" systems, but lacked experimental evidence so far.[1] While the ECD spectrum of $\mathbf{G_{BD}[2]}$ has the most intense Cotton band in the spectral area where the axis dominates the spectrum, in the two oligomers $\mathbf{G_{BD}[3]}$ and $\mathbf{G_{BD}[4]}$ the most intense Cotton band is found in the spectral area where the banister dominates the spectra. It has been previously observed, that in a series of chiral linear aromatic oligomers the chiroptical activity decreases, in contrast to helical conjugated systems where it increases.[24,26,27] Furthermore, they have the same cascade of Cotton bands, as has already been observed for oligoprolines[28] and enantiopure oligomeric helicenes.[29–31] Analysis of the computed transitions reveals that the non-linear increase in the molar ellipticity $\Delta\varepsilon$ (see Table 2) is probably stemming from a significant increase in the magnetic transition dipole moment; see the ESI† for a more detailed discussion.[26]

Table 2 Summary of the observed optical properties

	λ_{abs} [a]	λ_{em} [a] max	ϕ	$E_{0\text{–}0}$ [b]	ε [c]	$\Delta\varepsilon$ [c]	g_{abs} [c]
$\mathbf{G_{BD}[2]}$	386	395	0.5%	3.20	60×10^3	14	2.4×10^{-4}
$\mathbf{G_{BD}[3]}$	410	417	1.5%	3.00	59×10^3	44	1.1×10^{-3}
$\mathbf{G_{BD}[4]}$	420	427	1.5%	2.93	57×10^3	309	6.1×10^{-3}

[a] Wavelength in nm. [b] Energy in eV. [c] Molar absorption or ellipticity in M^{-1} cm^{-1}, respectively, read out for the most red-shifted local maximum (λ_{abs}).

Conclusion

In summary, a series of "Geländer" oligomers are reported giving access to systematic structure–property correlations enabled by using 90° rungs. The "Geländer" structures are created using a two-step assembly strategy. Beginning with a statistical end-capping oligomerization, which utilizes a Yamamoto-type coupling to form the axis. After the individual oligomers are chromatographically separated, an oxidative acetylene coupling is employed to arrange the helical banister. Individual enantiomers were isolated by HPLC on chiral stationary phases.

The identities of the structures are corroborated by NMR and optical spectroscopy, as well as mass spectrometry. Their spatial arrangement is elucidated by computational modeling and X-ray crystallographic data. The isolated enantiomers of the "Geländer" oligomers $\mathbf{G_{BD}[2]}$ to $\mathbf{G_{BD}[4]}$ are stable enabling the investigation of their length dependent (chir)optical properties. In spite of the small size of the series, the data display a promising increase in the molar elipticity with increasing length.

Our current focus is set on the optimization of the end-capped oligomerization strategy to assemble the heptamer, as modelling suggests that its banister completes a full helical turn which, besides the aesthetical appeal, would deepen our comprehension of size dependent properties of helically wrapped chromophores. In addition, we are exploring additional chromophores as potential subunits in the "Geländer" architecture, generalizing the approach that is reported here and tuning their optical properties *i.e.*, increasing the quantum efficiency.

Data availability

Synthetic procedures, analytical data, HPLC and GPC, chromatograms, and computational details are provided in the ESI.† (PDF) X-ray crystallographic data are provided for (*rac*)-$\mathbf{G_{BD}[3]}$ (CIF).

Author contributions

A. D'A. and M. M. conceived the project and wrote the manuscript together. M. M. supervised the project. A. D'A. carried out all experimental, spectroscopic, and computational work. C. C. E. K. helped in the purification and analysis by GPC and commented on the manuscript. D. H. performed advanced NMR spectroscopy and grew the single crystal of $\mathbf{G_{BD}[3]}$. O. F. and D. F. collected and refined the crystallographic data. All authors have given approval to the final version of the manuscript.

Conflicts of interest

There are no conflicts to declare.

Acknowledgements

The authors acknowledge generous support from the Swiss National Science Foundation (SNF Grant no. 200020-207744) and from the NCCR "Molecular Systems Engineering" (SNF Grant no. 51NF40-141825). M.M. acknowledges support from the 111 project (Grant No. 90002-18011002).

Notes and references

1 B. Kiupel, C. Niederalt, M. Nieger, S. Grimme and F. Vögtle, *Angew. Chem., Int. Ed.*, 1998, **37**, 3031–3034.
2 M. Rickhaus, L. M. Bannwart, M. Neuburger, H. Gsellinger, K. Zimmermann, D. Häussinger and M. Mayor, *Angew. Chem., Int. Ed.*, 2014, **53**, 14587–14591.
3 M. Rickhaus, M. Mayor and M. Juríček, *Chem. Soc. Rev.*, 2016, **45**, 1542–1556.
4 M. Modjewski, S. V. Lindeman and R. Rathore, *Org. Lett.*, 2009, **11**, 4656–4659.
5 M. Rickhaus, L. M. Bannwart, O. Unke, H. Gsellinger, D. Häussinger and M. Mayor, *Eur. J. Org. Chem.*, 2015, **2015**, 786–801.
6 M. Rickhaus, O. T. Unke, R. Mannancherry, L. M. Bannwart, M. Neuburger, D. Häussinger and M. Mayor, *Chem.–Eur. J.*, 2015, **21**, 18156–18167.
7 L. M. Bannwart, L. Jundt, T. Müntener, M. Neuburger, D. Häussinger and M. Mayor, *Eur. J. Org. Chem.*, 2018, **2018**, 3391–3402.
8 L. M. Bannwart, T. Müntener, M. Rickhaus, L. Jundt, D. Häussinger and M. Mayor, *Chem.–Eur. J.*, 2021, **27**, 6295–6307.
9 R. Mannancherry, M. Rickhaus, D. Häussinger, A. Prescimone and M. Mayor, *Chem. Sci.*, 2018, **9**, 5758–5766.
10 R. Mannancherry, T. Šolomek, D. Cavalli, J. Malinčík, D. Häussinger, A. Prescimone and M. Mayor, *J. Org. Chem.*, 2021, **86**, 5431–5442.
11 A. D'Addio, J. Malinčik, O. Fuhr, D. Fenske, D. Häussinger and M. Mayor, *Chem.–Eur. J.*, 2022, **28**, e202201678.
12 D. Vonlanthen, J. Rotzler, M. Neuburger and M. Mayor, *Eur. J. Org. Chem.*, 2010, **2010**, 120–133.
13 Y. Kozhemyakin, M. Krämer, F. Rominger, A. Dreuw and U. H. F. Bunz, *Chem.–Eur. J.*, 2018, **24**, 15219–15222.
14 S. Menning, M. Krämer, A. Duckworth, F. Rominger, A. Beeby, A. Dreuw and U. H. F. Bunz, *J. Org. Chem.*, 2014, **79**, 6571–6578.
15 H. Dekkiche, J. Malinčik, A. Prescimone, D. Häussinger and M. Mayor, *Chem.–Eur. J.*, 2021, **27**, 13258–13267.
16 E. L. Eliel, S. H. Wilen and L. N. Mander, *Stereochemistry of Organic Compounds*, Wiley, New York, 1994.
17 N. M. Jenny, M. Mayor and T. R. Eaton, *Eur. J. Org. Chem.*, 2011, **2011**, 4965–4983.
18 A. D'Addio, J. Malinčik, O. Fuhr, D. Fenske, D. Häussinger and M. Mayor, *Chem.–Eur. J.*, 2022, **28**, e202201678.
19 J. Crassous, M. J. Fuchter, D. E. Freedman, N. A. Kotov, J. Moon, M. C. Beard and S. Feldmann, *Nat. Rev. Mater.*, 2023, **8**, 365–371.
20 S. T. Bao, H. Jiang, Z. Jin and C. Nuckolls, *Chirality*, 2023, **35**, 656–672.
21 A. Chiesa, A. Privitera, E. Macaluso, M. Mannini, R. Bittl, R. Naaman, M. R. Wasielewski, R. Sessoli and S. Carretta, *Adv. Mater.*, 2023, **35**, 2300472.
22 P. Ludwig, F. Rominger, J. Freudenberg and U. H. F. Bunz, *Angew. Chem., Int. Ed.*, 2024, **63**, e202316902.
23 Y. Wu, J.-M. Han, M. Hong, M. D. Krzyaniak, A. K. Blackburn, I. R. Fernando, D. D. Cao, M. R. Wasielewski and J. F. Stoddart, *J. Am. Chem. Soc.*, 2018, **140**, 515–523.
24 H. Tanaka, Y. Inoue and T. Mori, *ChemPhotoChem*, 2018, **2**, 386–402.
25 L. Arrico, L. Di Bari and F. Zinna, *Chem.–Eur. J.*, 2021, **27**, 2920–2934.
26 C. Bræstrup, X. Xiao, F. García-González, T. Brock-Nannestad, D. Aranda, S. T. Bao, D. Cavlovic, H. Jiang, F. Ng, C. Nuckolls, F. Santoro and M. Pittelkow, *Adv. Opt. Mater.*, 2025, 2403061.
27 K. Takaishi, T. Yamamoto, S. Hinoide and T. Ema, *Chem.–Eur. J.*, 2017, **23**, 9249–9252.
28 S. Kakinoki, M. Kitamura, Y. Noguchi and Y. Arichi, *Pept. Sci.*, 2020, **112**, e24170.
29 C. Schaack, E. Sidler, N. Trapp and F. Diederich, *Chem.–Eur. J.*, 2017, **23**, 14153–14157.
30 C. Schaack, L. Arrico, E. Sidler, M. Górecki, L. Di Bari and F. Diederich, *Chem.–Eur. J.*, 2019, **25**, 8003–8007.
31 F. Furche, R. Ahlrichs, C. Wachsmann, E. Weber, A. Sobanski, F. Vögtle and S. Grimme, *J. Am. Chem. Soc.*, 2000, **122**, 1717–1724.